Journal of Photonics for Energy

PhotonicsforEnergy.SPIEDigitalLibrary.org

One-step, low-temperature deposited perovskite solar cell utilizing small molecule additive

Chun-Chao Chen
Zirou Hong
Gang Li
Qi Chen
Huanping Zhou
Yang Yang

SPIE.

One-step, low-temperature deposited perovskite solar cell utilizing small molecule additive

Chun-Chao Chen,[a] Zirou Hong,[a] Gang Li,[a] Qi Chen,[a,b] Huanping Zhou,[a,b] and Yang Yang[a,b,*]

[a]University of California, Department of Materials Science and Engineering, 420 Westwood Plaza Drive, Los Angeles, California 90095, United States

[b]University of California Los Angeles, California Nano Systems Institute, Los Angeles, California 90095, United States

Abstract. In the current study, the perovskite absorber ($CH_3NH_3PbI_3$) is processed via one-step deposition employing the small molecule additive, BmPyPhB, which can be dissolved in dimethylformamide along with precursors. Here, 1,3-Bis[3,5-di(pyridin-3-yl)phenyl]benzene (BmPyPhB) functions as the morphology controller to introduce an intermediate phase during perovskite film growth, which allows well-defined and precrystallized domains formed before the annealing treatment. Furthermore, a chloroform solvent wash procedure is applied afterward to remove BmPyPhB from perovskite without damaging the predetermined morphology. Thus, postannealing as low as 100°C for 5 min can achieve the optimal power conversion efficiency of 8% in a planar-structured inverted solar cell. © *2015 Society of Photo-Optical Instrumentation Engineers (SPIE)* [DOI: 10.1117/1.JPE.5.057405]

Keywords: perovskite; planar solar cell; solution process; small molecule additive; low temperature.

Paper 14083SS received Oct. 22, 2014; accepted for publication Dec. 17, 2014; published online Jan. 16, 2015.

1 Introduction

During the past year, perovskite solar cells have received great attention due to their efficiency advancement, mechanical flexibility, and solution coating capability.[1–5] Especially in the power-conversion efficiency improvement, perovskite solar cells have reached the 19% efficiency making it a great candidate for the next-generation, high-efficiency photovoltaic technology.[6] At the current stage, perovskite material, $CH_3NH_3PbI_3$, is the most commonly used sensitizer with a fixed energy bandgap of 1.52 eV and absorption range up to 800 nm.[7] One of the most common recipes in preparing $CH_3NH_3PbI_3$ ink for one-step coating was introduced by Graztel et al., using 1∶1 molar ratio of CH_3NH_3I (MAI) and PbI_2 in either dimethylformamide (DMF) or γ-butyrolactone.[8,9] Since then, the optimal morphology and device performances have been achieved by various processing approaches, such as substrate annealing, solvent removal, or solvent additive, in order to control crystal growth during spin coating.[10–13] Given that each of these approaches has its own unique morphology control mechanisms, there is still a lack of understanding on how to utilize the advantages of different approaches to achieve the optimal morphology of $CH_3NH_3PbI_3$ via a one-step solution method with a minimized thermal treatment.[14] Here, we presented a method to control the morphology of the perovskite absorber by adding a small molecule additive into its precursor solution in order to form a precrystallized intermediate state before the annealing step. Owing to the precrystallized film morphology, no prolonged thermal treatment at high temperatures is required for optimized device performance.

*Address all correspondence to: Yang Yang, E-mail: yangy@ucla.edu

2 Morphological Control of $CH_3NH_3PbI_3$

Figure 1(a) demonstrated a method of incorporating a small molecule, 1,3-Bis[3,5-di(pyridin-3-yl)phenyl]benzene (BmPyPhB), into the precursor solution (1 : 1 molar ratio of MAI and PbI_2) to retard the slow crystallization of large crystallites in the intermediate phase before thermal treatment and conversion to the $CH_3NH_3PbI_3$ perovskite phase. Here, BmPyPhB is selected according to its suitable solubility in both dimethylformamide (solvent for processing MAI : PbI_2) and chloroform (solvent for removing it after spin coating). The role of BmPyPhB can be described as the *in-situ* scaffold that occupies space during the film growth of perovskite. At the beginning, 3% (with respect to the total weight of PbI_2 and CH_3NH_3I) BmPyPhB is blended with the perovskite precursor in solution. Since BmPyPhB is inert, no chemical reaction or byproduct is expected between $CH_3NH_3PbI_3$ and BmPyPhB. Upon spin-coating and evaporation of the DMF solvent, BmPyPhB, owing to its planar structure as well as its pyridine ring, can quickly turn into small nanosized aggregates uniformly distributed in the precursor matrices. When the intermediate phase (MAI-PbI_2) starts to precipitate out, BmPyPhB aggregates, similar to the metal oxide scaffold, can provide numerous heterogeneous nucleation sites for the nearby precursor species to nucleate and crystallize rapidly. Since in the classical nucleation theory, the size of the crystal is inversely correlated to the number of nucleation sites, by providing sufficient heterogeneous nucleation sites, the resulting morphology of the intermediate phase should turn into a uniform and compact crystal domain. In the second step, BmPyPhB can be further removed by washing the film with one drop of chloroform (CF) solvent during high speed rotation. Since the precursor film is insoluble in CF, its structure is preserved. More importantly, the adverse effect of residual BmPyPhB trapped inside the perovskite sensitizer causing charge recombination can be minimized after CF washing.[11] Owing to the dense morphology of the intermediate phase, the morphology of the later perovskite phase can be equally dense and uniform after thermal treatment. Figure 1(b) also demonstrates the conventional spin-coating method and the speculated crystal growth for perovskite without the help of a small molecule

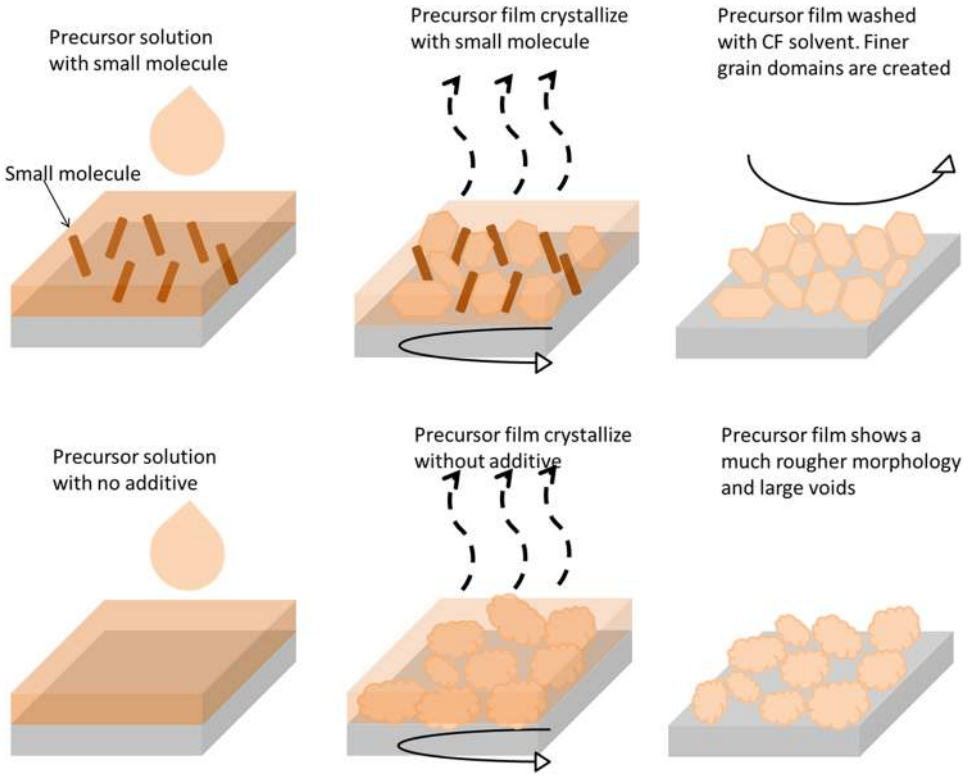

Fig. 1 (a) Solvent additive (small molecule) procedure for preparing the uniform and dense perovskite film and (b) regular procedure for preparing the perovskite film without additive. The resulting morphology is full of voids and not dense.

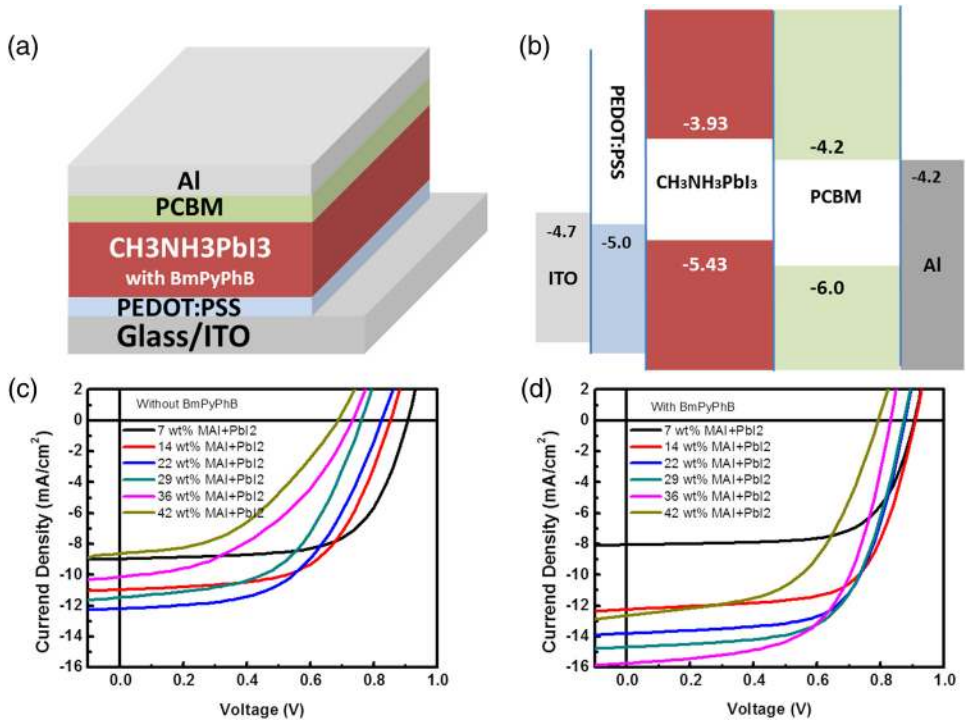

Fig. 2 (a) Device architecture of the planar structure perovskite solar cell (glass/ITO/PEDOT:PSS/perovskite layer/PCBM/Al); (b) proposed energy level landscape for perovskite solar cell; (c) $J-V$ curves for a planar junction cell processed without BmPyPhB; (d) $J-V$ curves for a planar junction cell processed with BmPyPhB.

additive. A rough, isolated, and void-presented morphology is expected for the nonmodified perovskite film.

Figures 2(a) and 2(b) show the device structure and energy level diagram for a planar-structured perovskite solar cell. The photocurrent density and voltage curve (J–V) for the perovskite solar cell in the planar junction are given in Figs. 2(c) and 2(d). A series of six different concentrations of precursor solution are used to deposit the perovskite sensitizer from BmPyPhB-modified and nonmodified precursor solutions. Based on different concentrations of the precursor ($MAI:PbI_2$), the resulting thickness of the spin-coated layer can be fine-tuned from 60 nm (7 wt.% of $MAI:PbI_2$) to 260 nm (42 wt.% of $MAI:PbI_2$). The summary of the performance parameters and thickness variations is listed in Table 1. The open-circuit voltage (V_{oc}) of the nonmodified samples shows a strong dependence on film thickness, possibly ascribed to the noncontinuous film morphology. The poor fill factor (FF) also indicates that the charge transport is possibly perturbed by the distorted crystal structure of perovskite. As the result, an unfavorable morphology obtained from nonmodified precursor solution makes the devices only efficient at a thin thickness (<100 nm). On the other hand, the BmPyPhB-modified samples show a great improvement to both V_{oc} and FF in device performance for all concentrations. The thickness tolerance of BmPyPhB-modified samples is enhanced to a 230-nm thickness making its light absorption much greater than that of nonmodified samples at a thin thickness. Moreover, the consistently high FF of BmPyPhB-modified samples at all thicknesses may also indicate a more organized and dense crystal structure which is beneficial to the charge extraction. Based on the above results, the effectiveness of using BmPyPhB as a structure modifier for perovskite has been validated through the photovoltaic performance shown above. An optimized power conversion efficiency (PCE) as high as 8.1% is demonstrated using a planar-structured solar cell. At the same time, the capability of BmPyPhB-modified samples to support a thick layer of perovskite at a relatively high efficiency also reinforces our claim that the role of a small molecule additive inside the precursor solution can be an effective morphology controller.

Figure 3 shows the atomic force microscopy (AFM) images corresponding to BmPyPhB-modified and nonmodified perovskite thin films at intermediate phase before applying thermal

Table 1 Photovoltaic performance of perovskite planar solar cells.

concen. (wt%)	thickness (nm)	V_{OC} (V)	J_{SC} (mA/cm^2)	FF	PCE (%)
$CH_3NH_3PbI_3$ planar junction (with no additive)					
7	60	0.90	8.9	0.66	5.28
14	105	0.86	11	0.60	5.67
22	142	0.82	12.1	0.55	5.45
29	180	0.76	11.5	0.54	4.71
36	230	0.74	10.1	0.43	3.21
42	265	0.68	8.6	0.44	2.57
$CH_3NH_3PbI_3$ planar junction (with BmPyPhB)					
7	60	0.90	8.05	0.69	4.99
14	105	0.90	12.2	0.67	7.35
22	142	0.88	13.8	0.65	7.89
29	180	0.88	14.7	0.63	8.14
36	230	0.84	15.7	0.60	7.91
42	265	0.80	12.6	0.54	5.44

annealing. From Figs. 3(a)–3(c), the nonmodified $CH_3NH_3PbI_3$ via the one-step solution method is characterized. Spin-coated from precursor concentrations ranged from 14, 29, to 42 wt.% of MAI:PbI_2, showing that the morphology of perovskite can behave quite differently. In the low concentration regime of 14 wt.% of MAI:PbI_2, the surface roughness of perovskite is confined with 10 nm in the height images and finer crystallite domain, with 100 nm is observed from the phase images. At this point, a few small voids are found and the film appearance right after perovskite deposition still remains transparent. As the concentration of the precursor reaches 29 wt.% of MAI:PbI_2 and above, a clear indication of needle-like crystallites and large voids can be found in height images. More importantly, the grain size also enlarges with increasing precursor concentration up to the submicrometer scale. Therefore, we speculate that when the precursor content in the solution is supersaturated (>29 wt.% of MAI:PbI_2), severe crystallization can happen instantly after the solution is dropped on the substrate. Because of the lack of the nucleation sites, crystallites tend to grow in a one-dimensional direction, resulting in a needle-like morphology.[13] Scanning electron microscopy (SEM) image taken after thermal annealing in Fig. 4(a) also confirms that large voids were formed. Although, in general the large grain size may be favorable for charge transport, the void and pin-hole that resulted from the noncontinuous film morphology is detrimental to the device performance and cannot be tolerated. The film appearance at this point is hazy and the rough surface of the intermediate phase of perovskite may also cause a problem for the surface coverage of PCBM on the top perovskite. Thus, the devices with the nonmodified one-step deposition method only function efficiently at low-concentration samples with a thin film thickness.

From Figs. 3(d)–3(f), the BmPyPhB-modified $CH_3NH_3PbI_3$ via the one-step solution method is characterized. The addition of BmPyPhB planarizes the surface roughness of perovskite making it free of large voids as shown in the samples with a concentration from 14 wt.% of MAI:PbI_2. At a high concentration regime (>29 wt.% of MAI:PbI_2), very few voids start to appear, explaining the small loss of V_{oc}. At the highest concentration of 42 wt.% of MAI:PbI_2, the resulting height image still shows that film morphology is continuous at most of the area with a slightly rougher surface. Based on these results, the given small molecule can allow the crystallites to grow in two-dimensional directions and cover up the whole surface area. Since there is a lack of needle-like crystallites, large voids are avoided and more uniform and compact grain

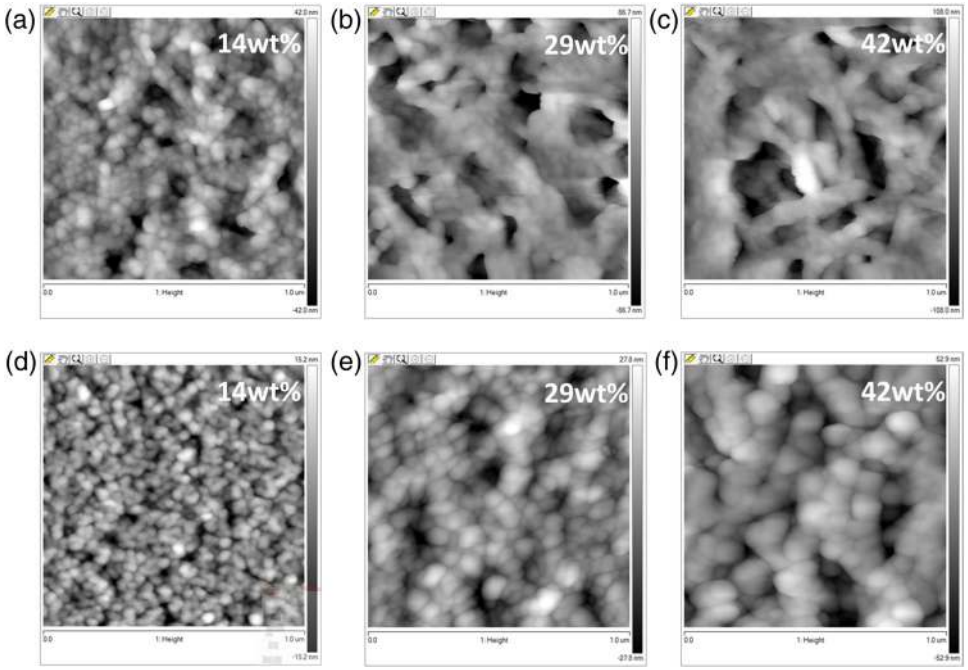

Fig. 3 AFM topography (prior to thermal annealing) of the perovskite film processed without BmPyPhB from (a) 14 wt%, (b) 29 wt%, (c) 42 wt%; similarly, AFM topography (prior to thermal annealing) of the perovskite film processed with BmPyPhB from (d) 14 wt%, (e) 29 wt%, (f) 42 wt%. The size of the AFM images is $1 \times 1\ \mu m^2$.

domains are observed for the precrystallized intermediate phase of perovskite film. The SEM image taken after thermal annealing in Fig. 4(b) also confirms that the majority of voids were removed. Furthermore, we also verify the outlook of the BmPyPhB-modified $CH_3NH_3PbI_3$ film to be transparent and at a minimal haze level indicating that the surface is smooth and less light is deflected. Owing to the continuous film morphology, samples modified with BmPyPhB can have a much better device performance at thick film thicknesses.

Furthermore, we took the external quantum efficiency (EQE) measurement for the optimized solar cell devices with and without the additive. The EQE measurements for each condition are provided in Fig. 5(a). The integrated current density from EQE is 11.2 mA/cm^2 for the devices without additive and 14.5 mA/cm^2 for the devices with the BmPyPhB additive, which are in good agreement with the J–V characteristics. The reduced current density in the case of non-additive samples can be ascribed to the decreased EQE response from a 600 to 800 nm wavelength. Since device samples without additive have a much rougher surface and hazy appearance,

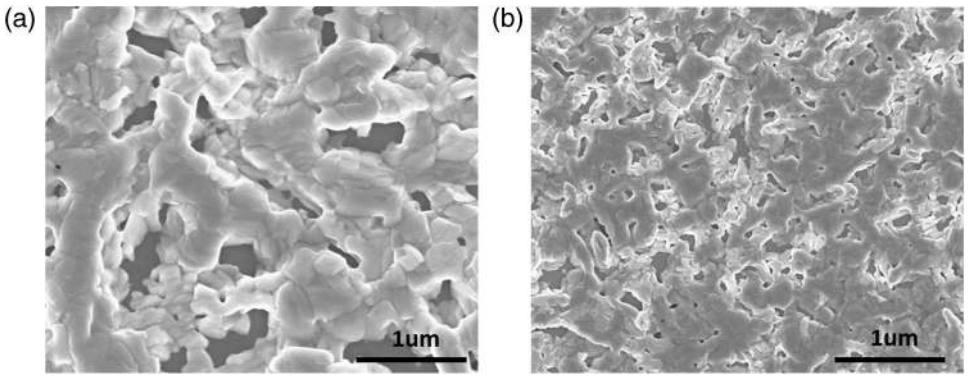

Fig. 4 SEM topography (taken after thermal annealing) of the resulting perovskite film processed without BmPyPhB (a) and with BmPyPhB (b) from 29 wt% precursor solution. The scale-bar of the SEM images is 1 μm.

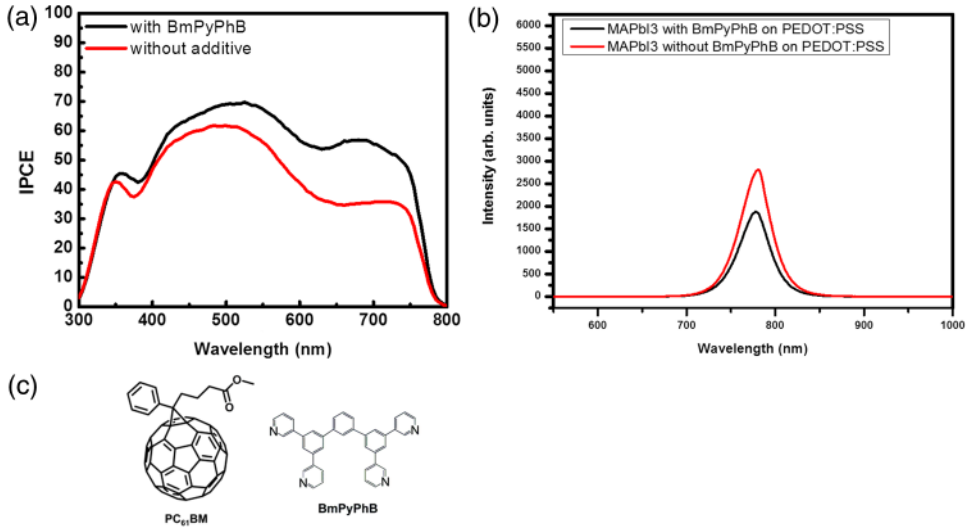

Fig. 5 (a) External quantum efficiency of the perovskite solar cell processed with and without BmPyPhB additive; (b) PL of perovskite film on PEDOT:PSS; and (c) chemical structures of PCBM, and BmPyPhB.

more deflected light beams at the long wavelength region can be expected, resulting in inferior absorption from 600 to 800 nm. Thus, surface planarization that again resulted from the morphological optimization is important to the device performance. Furthermore, in Fig. 5(b), photoluminescence (PL) measurement is performed on perovskite film with and without BmPyPhB. The result shows the more complete PL quenching in the case of perovskite film with BmPyPhB. This observation can be more evidence to support the improved photovoltaic performance in BmPyPhB-modified perovskite solar cells.

3 Experimentals

3.1 *Solar Cell Device Fabrication*

The device architecture of the planar junction cell is shown in Fig. 2(a). The devices were fabricated on ITO-coated glass substrates, with a sheet resistance of 15 Ω/square. The precleaned ITO substrates were treated with UV-ozone and then spin-coated with the PEDOT:PSS AI 4083 solution by baking at 140°C for 10 min in ambient air.[15,16] The samples were then transferred to a nitrogen-filled glove box for perovskite and PCBM [chemical structure provided in Fig. 5(b)] deposition. For perovskite, various thicknesses were deposited by spin-coating $CH_3NH_3I:PbI_2$ from 1:1 molar ratio in DMF solution with different concentrations at 4000 rpm for 10 s and a transparent intermediate phase was obtained. Different concentrations of solution were prepared by dissolving 18 mg of CH_3NH_3I and 52 mg of PbI_2 in 1 mL (7 wt.%) to 105 mg of CH_3NH_3I and 315 mg of PbI_2 in 1 mL (42 wt.%). For BmPyPhB [chemical structure provided in Fig. 5(c)] modified samples, a 3% BmPyPhB additive of 2.82 mg and 16.95 mg was added into 1 mL of the 7 wt.% and 42 wt.% solutions, respectively. Next, one drop of 20 μL clean CF solvent was dropped on the rotating sample at 5000 rpm to wash out the residual of the small molecule additive.[11] Samples were annealed at 100°C for 5 min.[13] The PCBM solution (1.0 to 1.5 wt.% in chlorobenzene) was spin-coated to form a 40 to 60 nm layer.[17] Last, 100 nm of Al was thermally evaporated through a shadow mask. The device area, defined by the overlap between the ITO and Al electrodes, was 0.100 cm^2.

3.2 *Solar Cell Device Measurement*

The current density–voltage (J–V) characteristic curve of solar cells was measured with a 0.1 cm^2 shadow mask using a Keithley 2400 source-meter under a simulated AM1.5G solar illumination from a Newport solar simulator setup. A KG-5 filter silicon photodiode was

used to calibrate the light intensity to 1 sun (100 mW/cm^2). To avoid overestimating the photocurrent, each device was completely isolated by scratching the surrounding films around the device.[18] EQEs were measured using an Enlitech QE-R spectral response measurement system. A SRC-2020 solar reference cell was used to calibrate the spectrum of EQE measurement. AFM and SEM measurements were performed at Nano & Pico Characterization Lab at California Nano Systems Institute and at Nanolab, respectively. The PL photons were counted by Picoharp 300 after preamplification by PAM102.

4 Conclusion

In conclusion, we have demonstrated an efficient approach to control the morphological growth of $CH_3NH_3PbI_3$ perovskite solar cells during the one-step deposition method. For a $CH_3NH_3PbI_3$ based absorber processed from CH_3NH_3I:PbI_2 precursor solution, a supersaturated solution at high concentration often produces needle-like morphology in the absence of scaffold materials to support uniform crystal growth. To solve this issue without the need for a metal oxide scaffold, a small molecule, BmPyPhB as the nanoscale scaffold, is added into the precursor solution to facilitate the 2-D growth of crystallites, leading to a continuous and dense morphology without large voids. BmPyPhB is removed later by clean CF solvent without disrupting the perovskite structure. With a fine morphology, a $CH_3NH_3PbI_3$ planar-structure solar cell sandwiched in between PEDOT:PSS and PCBM can attain 8.1% PCE. More importantly, we found such morphological control only requires a short thermal treatment of 100°C for 5 min to achieve the best performance. Our work not only presented an optimized device performance using small molecules as the processing additive but also can be seen as a promising solution for the later upscaling production of perovskite solar cells given its rapid thermal annealing advantage and simple device structure without a mesoporous metal oxide scaffold.

Acknowledgments

This work was financially supported by the Air Force Office of Scientific Research (AFOSR, Grant No. FA9550-09-1-0610), National Science Foundation (NSF ECCS-1202231), and UCLA internal funds. The authors would like to thank Dr. Jing Gao for AFM measurement and C.C.C. would like to thank NSF-funded IGERT: Clean Energy for Green Industry Fellowship (Grant DGE-0903720).

References

1. A. Kojima et al., "Organometal halide perovskites as visible-light sensitizers for photovoltaic cells," *J. Am. Chem. Soc.* **131**, 6050–6051 (2009).
2. M. M. Lee et al., "Efficient hybrid solar cells based on meso-superstructured organometal halide perovskites," *Science* **338**, 643–647 (2012).
3. J. Burschka et al., "Sequential deposition as a route to high-performance perovskite-sensitized solar cells," *Nature* **499**, 316–319 (2013).
4. J. H. Heo et al., "Efficient inorganic-organic hybrid heterojunction solar cells containing perovskite compound and polymeric hole conductors," *Nat. Photonics* **7**, 486–491 (2013).
5. M. Liu, M. B. Johnston, and H. J. Snaith, "Efficient planar heterojunction perovskite solar cells by vapour deposition," *Nature* **501**, 395–398 (2013).
6. H. Zhou et al., "Interface engineering of highly efficient perovskite solar cells," *Science* **345**, 542–546 (2014).
7. J.-H. Im et al., "6.5% efficient perovskite quantum-dot-sensitized solar cell," *Nanoscale* **3**, 4088–4093 (2011).
8. H.-S. Kim et al., "Lead iodide perovskite sensitized all-solid-state submicron thin film mesoscopic solar cell with efficiency exceeding 9%," *Sci. Rep.* **2** (2012).
9. L. Etgar et al., "Mesoscopic $CH_3NH_3PbI_3/TiO_2$ heterojunction solar cells," *J. Am. Chem. Soc.* **134**, 17396–17399 (2012).
10. J. Y. Jeng et al., "$CH_3NH_3PbI_3$ perovskite/fullerene planar-heterojunction hybrid solar cells," *Adv. Mater.* **25**, 3727–3732 (2013).

11. N. J. Jeon et al., "Solvent engineering for high-performance inorganic–organic hybrid perovskite solar cells," *Nat. Mater.* **13**, 897–903 (2014).
12. P. W. Liang et al., "Additive enhanced crystallization of solution-processed perovskite for highly efficient planar-heterojunction solar cells," *Adv. Mater.* **26**, 3748–3754 (2014).
13. M. Xiao et al., "A fast deposition-crystallization procedure for highly efficient lead iodide perovskite thin-film solar cells," *Angew. Chem.* **126**, 10056–10061 (2014).
14. J. M. Ball et al., "Low-temperature processed meso-superstructured to thin-film perovskite solar cells," *Energy Environ. Sci.* **6**, 1739–1743 (2013).
15. C. C. Chen et al., "Visibly transparent polymer solar cells produced by solution processing," *ACS Nano* **6**, 7185–7190 (2012).
16. C.-C. Chen et al., "High-performance semi-transparent polymer solar cells possessing tandem structures," *Energy Environ. Sci.* **6**, 2714–2720 (2013).
17. C. Zuo and L. Ding, "An 80.11% FF record achieved for perovskite solar cells by using the NH 4 Cl additive," *Nanoscale* **6**, 9935–9938 (2014).
18. C. C. Chen et al., "An efficient triple-junction polymer solar cell having a power conversion efficiency exceeding 11%," *Adv. Mater.* **26**, 5670–5677 (2014).

Biographies of the authors are not available.